Optical feedback implementation for polymer based tunable laser

Master's Thesis of

Tianwen Qian

at the Karlsruhe School of Optics & Photonics
in cooperation with Fraunhofer Heinrich-Hertz-Institut

Reviewer:	Prof. Dr. Bryce S. Richards
Second reviewer:	Dr. Ulrich W. Paetzold
Advisor:	David de Felipe Mesquida

July 2018 – December 2018

Karlsruhe Institute of Technology
Karlsruhe School of Optics & Photonics
Schlossplatz 19
76131 Karlsruhe | Germany

I herewith declare that the present thesis is original work written by me alone, that I have indicated completely and precisely all aids used as well as all citations, whether changed or unchanged, of other theses and publications, and that I have observed the KIT Statutes for Upholding Good Scientific Practice, as amended.

Karlsruhe, 30.12.2017

. . . . . .

(Tianwen Qian)

Abstract

The optical feedback introduced improvement on laser linewith and bandwidth has drawn a significant interest for the researchers.

In practice external feedback when coupled into the laser cavity through the output facet, causes a modification of the photon density. This perturbation leads to a fluctuation in the carrier density affecting the optical gain. Since the fluctuations of optical refractive index are directly related to the carrier density [11], the external feedback also introduces phase fluctuations. The interaction of the intensity and phase fluctuations makes the dynamics of the laser system under self-injection very complex leading to system instabilities and even chaos. [Kechaou, Grillot et al 2012]

As high-speed fiber-optic communication becomes increasingly important, so does the need to perform precision measurements on lasers and lightwave systems.

Contents

1. Introduction

The focus of this thesis is the study of the optical feedback effects on polymer-based tunable laser in order to improve its performance in linewidth and bandwidth. The tunable laser is constructed by a hybrid approach combining polymer-based photonic integrated circuits (PIC) and active Indium Phosphide (InP) components.

Coherent optical communication systems are gaining rapid importance because they allow to increase the speed (data rate) of transmission, by making use of the phase-predicatability of lasers with narrow spectral linewidth.

Semiconductor laser diodes with wide direct modulation bandwidth represent a relevant element to fulfill the continuously increasing need for low-cost optical communications systems with high bit-rate.

The directly modulated laser is a simple and reliable source for high speed optical information transmis- sion. It is especially useful in medium to short distance applications (e.g. local area networks and optical interconnects) where the excess pulse dispersion due to laser chirp is not a critical issue. The laser modulation response can in most cases be described with a three pole transfer function.' The modulation bandwidth is then determined by the maximum achievable resonance frequency, the damping of the resonance peak and possible additional parasitic-like effects due to contact parasitics or diffusion-limited transport through the separate confinement layers.' For FP-lasers and single section DFB-lasers it is found both theoretically and experimentally that the damping of the relaxation peak increases approximately linearly with the relaxation frequency squared and this relation leads to an ultimate limit of the modulation response that mainly is determined by the ratio between the nonlinear gain coefficient and differential gain coefficient of the active material.2 However, this is not true in DBR-lasers or inhomogenously pumped multi-section DFB-lasers where it can be shown that the dispersive effects of the Bragg grating can alter both the frequency of the relaxation peak and its damping.

For the design process a set of three masks is needed, corresponding to the electrode, waveguide and air trench geometry.

The goal of this work is to analyze and improve the characteristics of the laser under feedback condition. Parameters measured by different set-ups for the characterization are presented in **??**. The samples produced based on this work are then characterized using optical transmission and reflection measurements. The measurements of these lasers, consisting of testing the designs, the application of different tuning principals and tuning experiments, are presented.

2. Theory of Laser Coupled with Passive Cavity

Semiconductor lasers with external cavities exhibit a variety of dynamical phenomena, depending on key parameters, comprising feedback strength, feedback delay, pump current, feedback type, and laser nonlinearity [1]. Among all of them, the feedback sensitivity of laser diodes is governed essentially by the feedback parameters C, X and κ_{ext}. In order to correctly consider the feedback effect in our tunable DBR laser, a three-mirror laser model and its equivalent two-mirror Fabry-Perot cavity are considered in Figure 2.1.

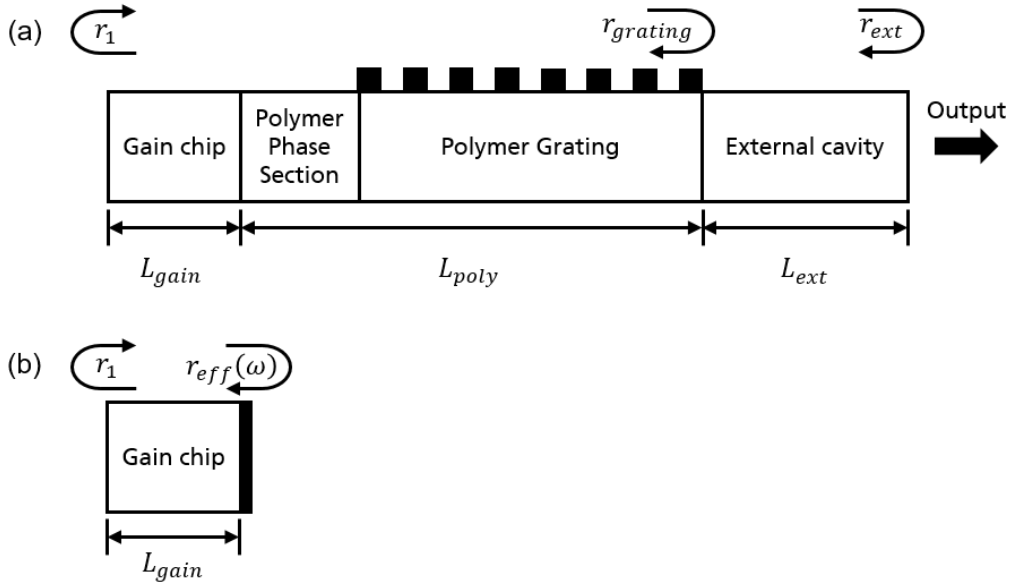

Figure 2.1.: (a) DBR laser with external cavity and (b) its equivalent cavity with effective mirror to model the feedback effect. The InP gain section that possesses a length of L_{gain} is equipped with a high reflection (HR) front facet and is butt-coupled to the Polyboard. The Polyboard consists up of a phase and grating section with a total length of L_{poly}, the external cavity is also on the Polyboard with a length of L_{ext} after the grating section. r_1, $r_{grating}$ and r_{ext} are amplitude reflectivities of the gain chip front facet, grating and external reflector respectively.

The feedback coefficient, C, characterizes the level of feedback in relation to how it affects the mode structure of the laser, is defined as

$$C = X\sqrt{1+\alpha^2} \tag{2.1}$$

with

$$X = \frac{\tau_{ext}}{\tau_{gain} + \tau_{poly}} \kappa_{ext} \tag{2.2}$$

$$\kappa_{ext} = \frac{r_{ext}}{r_{grating}} \left(1 - \left|r_{grating}\right|^2\right) \tag{2.3}$$

where $\tau = 2nL/c$ is the roud trip time in the corresponding section, κ_{ext} is the coupling coefficient from the grating reflector to the external cavity and α is the linewidth enhancement factor. Note that here the grating reflectivity $r_{grating}$ is considered as a static value, which leads to a effective grating length $L_{eff} = tanh(\kappa L)/2\kappa$ shorter than the real grating length L [2]. The L_{eff} is then contained in the normal cavity and the rest of the grating is included in the external cavity.

The C parameter indicates the laser stability under feedback is affected both by external reflector r_{ext} and external round-time delay τ_{ext}. When $C < 1$, usually for weak feedback and relatively short external cavities, the laser operates in a single mode lasing region and is phase dependent to the external feedback, when $C > 1$, over one stable mode will appear and the laser will undergo a route-to-chaos behavior until it reaches coherence-collapse [3] region, which is the region IV for the experimentally identified five distinct regimes of laser performance under feedback [4]. After the coherence-collapse region, if the feedback strength is even higher, the laser will become stable single mode again lasing with the compound cavity mode.

It is useful to identify the static lasing behavior by using C parameter, but in order to quantitatively model the laser under feedback, the equivalent two-mirror Fabry-Perot cavity by replacing the external feedback part with an effective mirror of reflectivity $r_{eff}(\omega)$ is considered

$$r_{eff}(\omega) = r(\omega)e^{-i\varphi(\omega)} = \frac{r_{grating}(\omega) + r_{ext}W}{1 + r_{grating}(\omega)r_{ext}W} \tag{2.4}$$

$$W = e^{-2\alpha_{poly}L_{ext}} e^{-2i\beta_{poly}L_{ext}} \tag{2.5}$$

where α_{poly} and β_{poly} are the propagation loss and the propagation constant of the external cavity respectively, $r_{grating}(\omega)$ is the frequency-dependent complex amplitude reflectance of the grating reflector [5].

The resonance equation G for the effective laser cavity model is then given by [6]

$$G = r_1 e^{-2i\tilde{\beta}_{gain}L_{gain}} r_{eff}(\omega) = |G|e^{i\varphi(\omega)} \tag{2.6}$$

with

$$\tilde{\beta}_{gain} = \beta + i\beta_i = \beta + \frac{i}{2}(g - \alpha_i) \tag{2.7}$$

where the real part $\beta = 2\pi n_{gain}/\lambda$ is the propagration constant inside the gain section, and the imaginary part consists of the modal gain g and the internal loss α_i in the gain medium [7]. Cavity modes are obtianed from Equation 2.6 for integer values of $\varphi/2\pi$; for the lasing mode m at threshold we have

$$|G(\lambda_m)| = G_m = 1, \ \varphi_m = 2m\pi \tag{2.8}$$

these two conditions allow to numerically find the lasing mode wavelength λ_m.

2.1. Linewidth and Chirp Reduction

Linewidth and chirp reduction due to the optical feedback is related to the factor F, which is given as [8]

$$F = 1 + A + B \tag{2.9}$$

with

$$A = \frac{1}{\tau_{gain}} \frac{d\varphi_{r_{eff}}}{d\omega} \tag{2.10}$$

$$B = \frac{\alpha}{\tau_{gain}} \frac{d \ln r_{eff}}{d\omega} \tag{2.11}$$

$$\Delta\omega = \frac{\Delta\omega_0}{F} \tag{2.12}$$

$$\Delta\nu = \frac{\Delta\nu_0}{F^2} \tag{2.13}$$

where α is the linewidth enhancement factor, $\Delta\omega$, $\Delta\nu$ and $\Delta\omega_0$, $\Delta\nu_0$ are the chirp and linewidth with and without feedabck respectively. The parameter A is the freqeuncy derivative of the r_{eff} phase in Equation 2.4, it denotes the ratio of the effecitve round trip time (cavity path length outside gain medium) to the roun trip time in the gain section (gain section path length). It can be interperate as the ratio of the photon numbers outside to inside the gain medium, which remains nearly constant once the laser cavity is formed. By designing a cavity with a long external cavity, a large A can be achieved. However, parameter B, representing the slope of the spectral reflectivity, is changed if the lasing mode is detuned. Additional reduction occurs only at the rising slope of the spectral peak of the external feedback which represents the contribution of the detuned loading effect and will be explained in Subsection 2.2.1.

Consider the five different feedback regions studied in [4], the reduction factor at weak feedback ($C < 1$) becomes [7, 9]

$$F = 1 + C\cos(\phi_{ext} + \arctan\alpha) \tag{2.14}$$

where $\phi_{ext} = 2\beta_{poly}L_{ext}$ is the round trip phase of the external cavity. Equation 2.14 shows that at weak feedback, the linewidth can either be narrowed $\Delta\nu_0/(1+C)^2$ or broadened $\Delta\nu_0/(1-C)^2$ depending on the feedback phase. For strong feedback, which is more interesting and stable for the practical implementation, the factor F becomes

$$F = 1 + f_{ext}\frac{\tau_{ext}}{\tau_{gain} + \tau_{poly}} \tag{2.15}$$

with

$$f_{ext} = \eta_{couple}R_{ext} \tag{2.16}$$

where η_{couple} is the coupling coefficient between the normal cavity and external cavity. This parameter is included because for the design presented in Section 4.1, the feedback from the external cavity is not totally coupled back to the normal cavity. However for the case considered here, $\eta_{couple} = 1$.

According to Equation 2.14 and Equation 2.15 we calculated the linewidth reduction factor F^2 versus the external cavity length as shown in Figure 2.2. L_c indicates the length when the C parameter goes over 1 where unstable laser behavior is expected. Figure 2.2 is caculated under the configuration that the feedback comes from the chip edge, which is form by a polymer/air interface and it leads to $R_{ext} = 0.187$.

Table 2.1.: Parameters used for linewidth reduction factor F^2 calculation.

Symbol	Description	Value
L_{gain}	Active section length	300 μm
L_{phase}	Phase section length	525 μm
$L_{grating}$	Grating section length	699.84 μm
L_{poly}	Polymer section length	1224.84 μm
α	Linewidth redcution factor	-3
$R_{grating}$	Grating reflectivity	0.3
R_{ext}	External cavity reflectivity	0.187

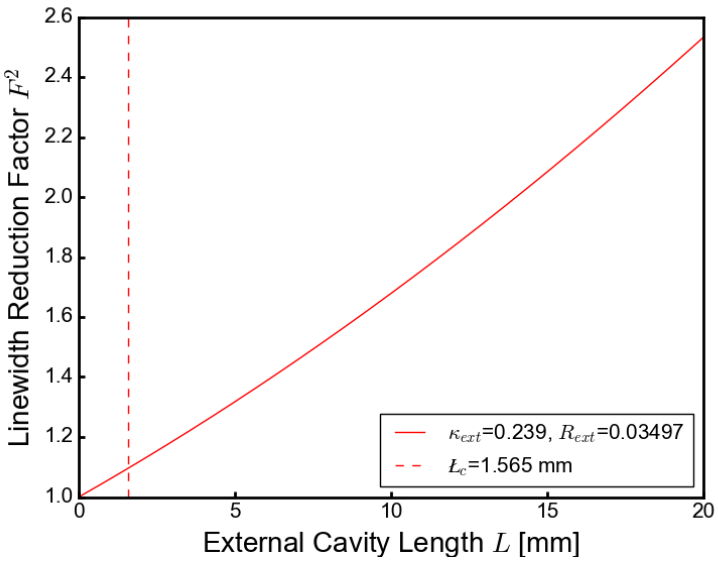

Figure 2.2.: Calculated linewidth reduction factor F^2 consider the feedback comes from the poly/air interface. L_c indicates the length when the C parameter goes over 1 where unstable laser behavior is expected.

2.2. Bandwidth Enhancement

The maximum bit rate achieved by direct modulated lasers is limited by the well known resonance between carriers and photons [7]. Many solutions have been proposed to over-

come this restriction and three approaches to achieve broader bandwidth are explored in detail here.

2.2.1. Detuned Loading Condition

The first mechanism identified to extend the modulation bandwidth of a semiconductor laser is the detuned loading effect which is due the dispersion effect introduced by a coupled cavity [10, 11] or by a distributed mirror (e.g. DBR [12, 13, 14]). It can be achieved when positioning the lasing mode at a slightly higher wavelength respect to the minimum threshold gain condition, which means the lasing mode of a DBR laser is oscillating at the higher slope of its grating response. It is reported that when the laser is operating at the longer wavelength side, the enhancement of modulation speed, reduction of phase noise (linewidth), and suppression of FM modulation (chirping) can be achieved [10]. The detuned loading of the laser cavity increases the interaction between the photons and the free carriers in the laser cavity which will both increase the modulation bandwidth and reduce the variation of the carrier density during modulation [15]. This is because, in the longer wavelength region, the increase of the carrier density increases the material gain while reducing the mirror loss (i.e. increase the reflection from the grating). As a result, the effective differential gain is increased, which, in turn, reduces the effective linewidth enhancement factor [10, 14].

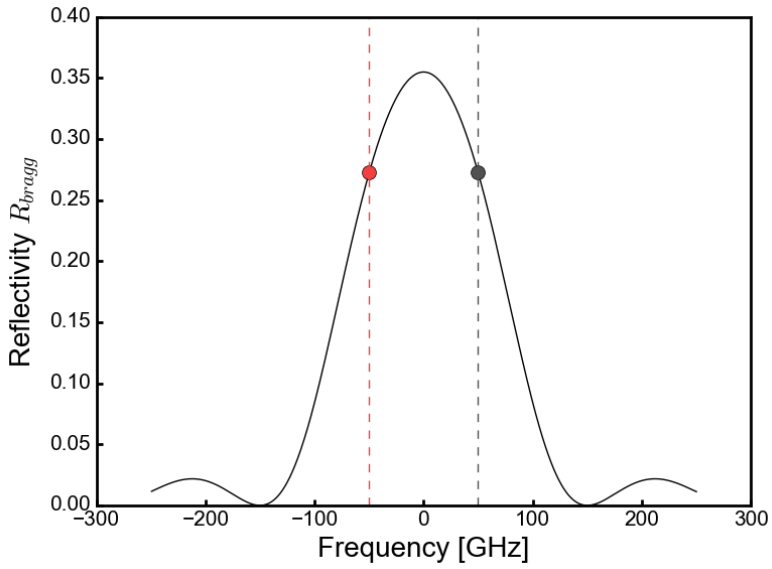

Figure 2.3.: Detuned loading condition with respect to the grating response. The red and grey dots correspond to the lasing mode detuend to the longer and shorter wavelength sides.

2.2.2. Undamped Relaxation Oscillation

Relaxation oscillation in a semiconductor laser occurs because the carrier cannot follow the photon decay rate, it usually smoothly decays out as long as the disturbance (e.g. external feedback) is small enough [16]. However, it can become undamped when the laser is influenced by strong feedback (e.g. from the chip facet), which affects the laser lorentzian lineshape that the undamping peaks appear beside the main mode with the mode spacing of relaxation frequency in the spectrum. The undamped relaxation oscillation occurs for the appropriate combinations of feedback phase and strength as shown in Figure 2.4. The satellite peaks first show up with low phase current, then slowly increase their intensity and move towards the main peak, following with more satellite peaks appearing when the corresponding relaxation oscillation frequency is decreasing.

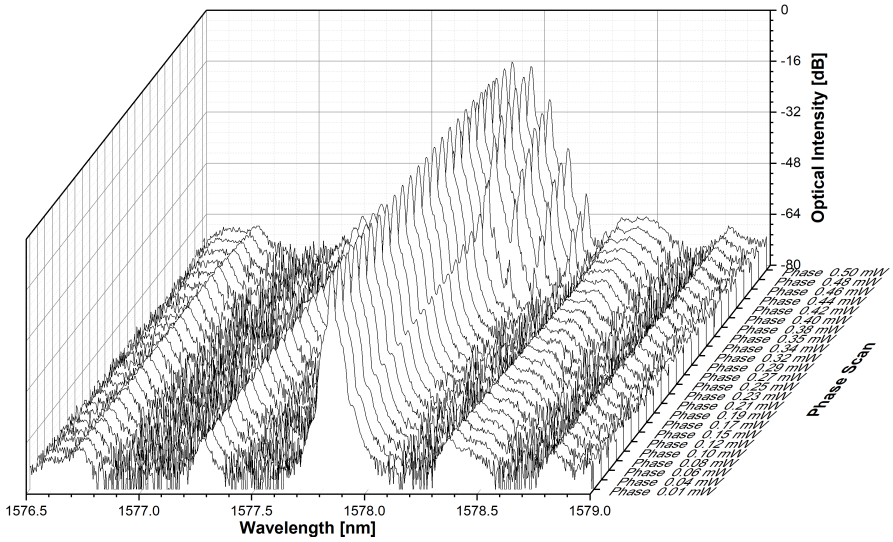

Figure 2.4.: Phase scan of the tunable DBR laser spectra with feedback from chip facet. The side peaks of undamped RO start to appear with increasing of their intensity and shifting towards the main peak. While the applied phase current keep changing, more peaks show up until the laser shift to another mode and becomes stable single mode lasing again.

Since the incoming feedback acts like a perturbation for the normal laser which introduces the amplitude modulation, the undamped RO can be also called as self-modulation or self-pulsation. The mechanism of self-pulsation is analysed and discussed in [17] as "dispersive Q-switching". In order to explain the self-pulsations one usually assumes some kind of a Q-switching process, where the term Q-switching denotes a switching of the quality-factor of the laser cavity. If an increase of optical power yields a decrease of optical loss (or an increase of optical gain) within the laser, the round trip gain may become larger than unity, yielding an exponential increase of optical power, corresponding to the rising edge of a developing pulse. On the other hand an increased power yields an increasing consumption of carriers so that finally the carrier density is too low to maintain a unity round trip gain and therefore the optical power collapses. A recovery time is required in order to increase the carrier density again until the next pulse develops. The

repetition frequency for these pulses is of the same order as the relaxation resonance frequency [9]. The bandwidth enhancement by the self-pulsation effect has beed reported as a clear undamping of the relaxation peak which in some cases ultimately led to self-pulsations at the relaxation frequency is observed in the small signal modulation response of the laser. The increased relaxation frequency and the undamping of the relaxation peak can be utilised in ordre to achieve higher bandwidth [18].

2.2.3. Photon-Photon Resonance

Another approach used to extend the dynamic properties of an integrated laser is similar to detuned loading condition but in addition it takes advantage of the interaction between the lasing mode and an adjacent longitudinal cavity mode, properly separated in frequency in such a way they can interact due to the carrier pulsation introduced by the applied modulation signal at the gain section. This interaction introduces a resonance in the impulse modulation (IM) response at the frequency corresponding to the modes separation. This resonance is frequently called Photon-Photon resonance (PPR), to distinguish this interaction mechanism respect to the Carrier-Photon resonance (CPR) [19]. The appearing of the PPR should not be too far away from the relaxation oscillation frequency so that the dip in between two peaks will not be deep enough to reach the -3 dB limation in the modulation response as shown in Figure 2.5.

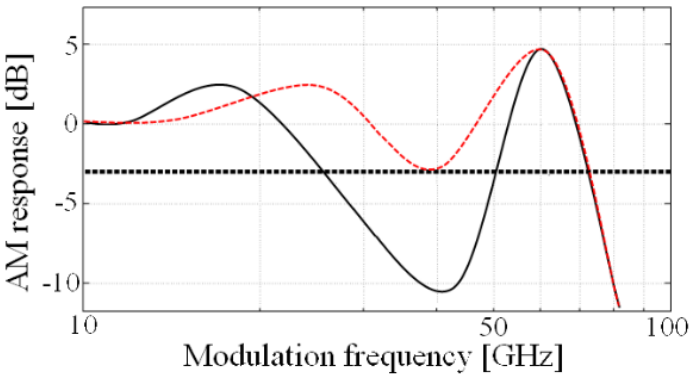

Figure 2.5.: Example of modulation responses obtained in cavity exploiting the PPR effect. The black line indicates a case in which the CPR and the PPR peaks are too much separated whereas in the case indicated by the red line the modulation bandwidth extension is achieved [19].

The large enhancement of the modulation bandwidth, has been already observed to be closely related to a special behavior of the cavity Round Trip Phase (RTP) function [20], which is the phase factor $\varphi(\omega)$ in Equation 2.6. In order to illustrate the operation principle of the PPR, we did the calculation by taking the simplified DBR laser structure as in [19], which contains only a gain section and a grating. The parameter used for calculation is shown in Table 2.2. The python code used for calculation is provided in Section A.1.

The caculated result is shown in Figure 2.6. The most favorable operation condition is when the lasing mode f_0 operates in the detuned loaidng condition $f_0 < f_B$, a mode

Table 2.2.: Simplified DBR laser cavity parameters used for calculation [19].

Symbol	Description	Value
L_A	Active region length	140 μm
L_G	Grating region length	780 μm
κ	Grating coupling coefficient	20 cm^{-1}
n_{eff}	Effective refractive index	3.7
R_R	Right side reflectivity	0
R_L	Left side reflectivity	0.32

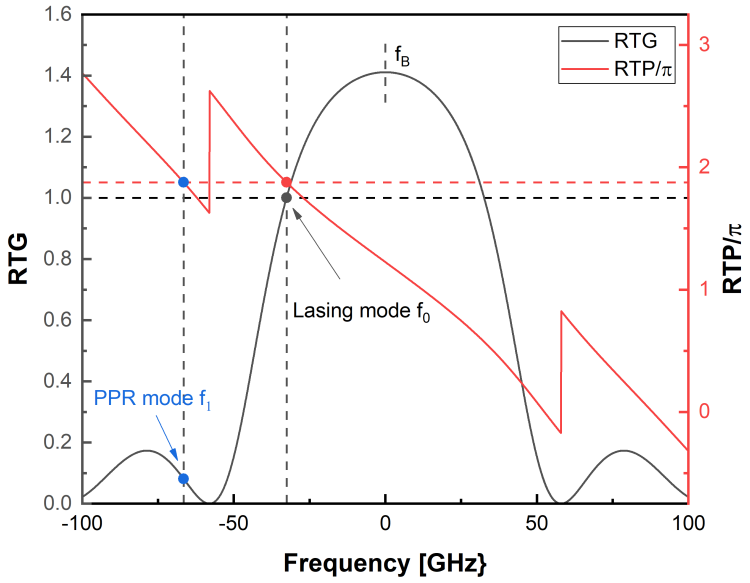

Figure 2.6.: Round trip gain (RTG, grey curve) and phase (RTP, red curve) functions computed at the DBR threshold. The grey and red marker represent the lasing mode f_0 at the corresponding RTG and RTP curve, the blue marker indicates the PPR mode f_1.

on the same side respect to the Bragg wavelength f_1 is placed on the the first lobe of the Round Trip Gain (RTG) curve. In this mode configuration, the PPR effect can arise due to the coupling between mode f_0 and f_1 [19], the corresponding PPR frequency is then the difference freqeuncy between the lasing mode f_0 and the PPR mode f_1. In order to generate an adjacent longitudinal cavity mode under feedback, a strong feedback condition is required, which will form compound cavity modes with the free spectral range (FSR) contains the normal cavity plus the external cavity as shown in Equation 2.17

$$\Delta\nu = \frac{c}{2(n_{gain}L_{gain} + n_{poly}L_{eff})} \tag{2.17}$$

this equation is also used as the design guideline in Section 4.1.

3. Tunable Laser with Reflection from Chip Facet

Characterization of the normal tunbale DBR laser linewidth, RIN, bandwidth, α parameter and phase noise are measured with (1) Cleaved fiber with oil and (2) Lensed fiber, which corresponding to the laser without feedback and with feedback from chip facet conditions. Principle of each measurement will be introduced and the results will be compared in the following sections.

The measurements are done by fixing the gain section current at $I_{gain} = 80\ mA$, grating section current at $I_{grating} = 15\ mA$ and scanning the phase section from 0 mA to 30 mA with the step of 0.5 mA, each current step is considered as one index which leads to in total of 61 index numbers. The principle of phase scan and the observed spectra are shown in Figure 3.1 and Figure 3.2. By tuning the phase through the increasing current it shifts the cavity modes toward the shorter wavelength side, this effect is done by change of the effective refractive index inside the polymer waveguide which in turn changes the effecitve optical length of the cavity. From the design parameters we caculated the mode spacing for normal cavity and external cavaity as $\Delta\nu_{cavity} = 67.04\ GHz$ and $\Delta\nu_{ext} = 56.35\ GHz$ respectively. As seen from Figure 3.2 (a), the laser initially operates in the region where the external cavity dominates, it is because with the feedback from the chip facet, the laser works in the strong feedback region. While shifting the phase current, the undamped RO starts to appear as shown in Figure 2.4 and Figure 3.2 (b).

The scanning of the spectra and the examing of the side mode suppression ratio (SMSR) are shown in Figure 3.3. Due to the hysteresis effect the laser wavelength has a little shift under these two configurations, e.g. the mode hopping point in Figure 3.3 a) appears at index 51 and the correspoinding point in Figure 3.3 (b) is at index 48. Besides, the additional hopping behavior in Figure 3.3 (b) is due to the feedback effect since the undamped RO peaks appearing in the spectra. Important to note that the light grey points marked at the beginning of Figure 3.3 (c) are unstable working points with SMSR lower than 40 dB, several modes appeared at these phase currents and the laser performance dropped drastically, which can be seen from the α-factor measurement in Section 3.4.

Regarding to the cavity mode shifting behavior, we think

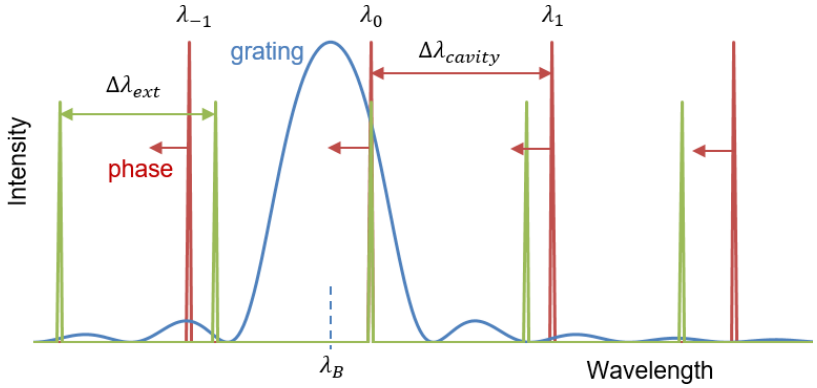

Figure 3.1.: Principle of phase scan in tunable DBR laser. Red and green curves represent the mode of the normal cavity and external cavity respectively. The different intensity is under the consideration that usually the feedback power is less than the output power. λ_0 is the lasing mode, λ_{-1} and λ_1 are its adjacent modes. λ_B is the Bragg wavelength which indicates the center of the grating response. $\Delta\lambda_{cavity}$ and $\Delta\lambda_{ext}$ are the mode spacing of the normal cavity and the external cavity. The red arrow indicates the phase shifts the cavity modes toward the shorter wavelength through the increasing phase current.

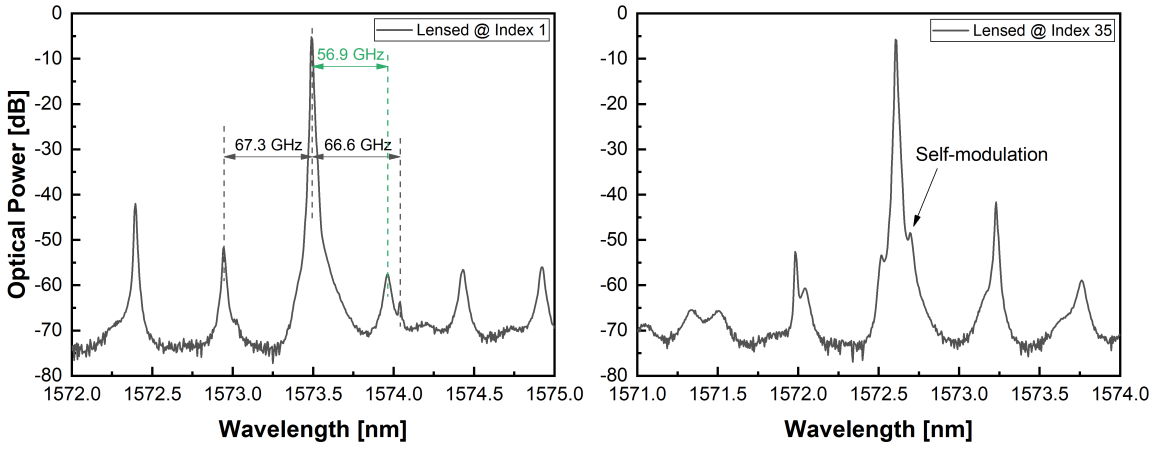

Figure 3.2.: Observed spectra for different phase current (index).

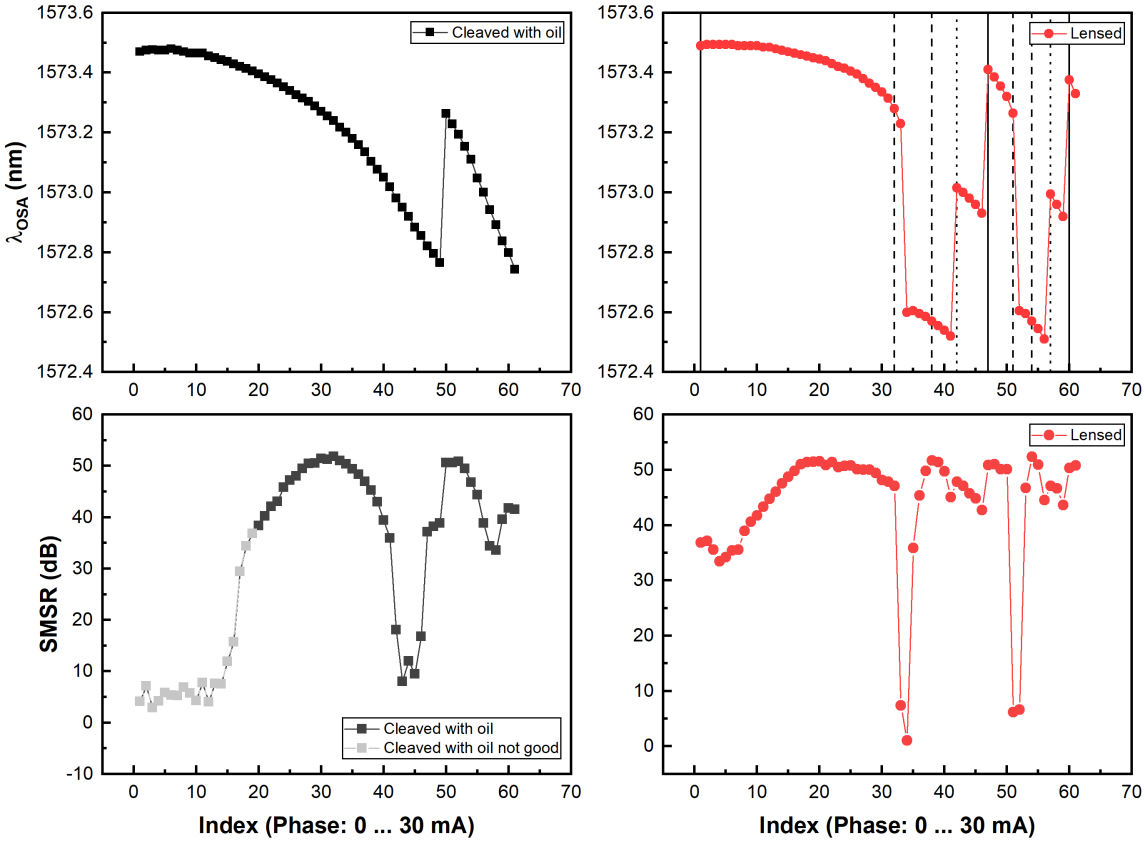
Cleaved with oil
Lensed
λOSA (nm)
SMSR (dB)
Cleaved with oil
Cleaved with oil not good
Index (Phase: 0 ... 30 mA)
Index (Phase: 0 ... 30 mA)

Figure 3.3.:

3.1. Linewidth Measurement

Laser linewidth is measured by self-homodyne method in the characterization. Self-homodyning can be described mathematically as a single-delay autocorrelation, which is shown in Figure 3.4, the optical spectrum at f_0 autocorrelates with the delayed version of itself to produce a time-fluctuating spectrum, whose detected voltage has a power spectrum centered at zero frequency. For the case of a laser with Lorentzian lineshape, the half-width of the detected spectrum is equal to the linewidth of the laser.

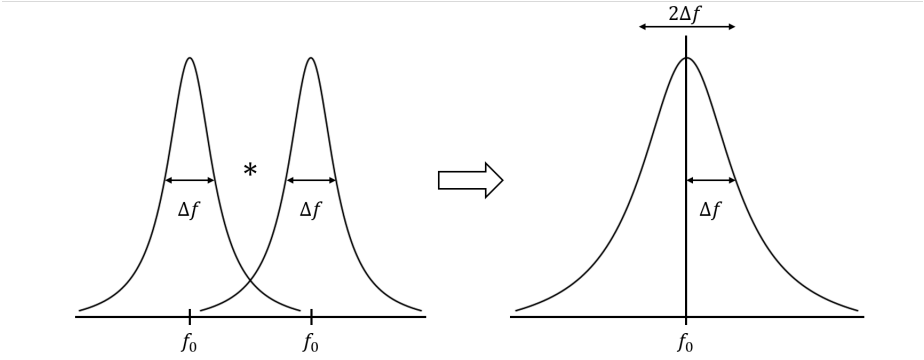

Figure 3.4.: Linewidth of a DBR laser using the self-homodyne technique. The optical spectrum at f_0 autocorrelates with the delayed version of itself to produce a time-fluctuating spectrum, whose detected voltage has a power spectrum centered at zero frequency, the half-width of the detected spectrum is equal to the linewidth of the laser.

The self-homodyne measurement set-up is shown in Figure 3.5. The input directional coupler of the interferometer splits the light from the laser into two paths. One path is delayed in order to decorrelate the combinning signals, P_1 and P_2. The output coupler combines the two signals, which are then mixed at the photodectector of the lightwave signal analyzer. The homodyne power spectrum is then observed on the analyzer from which the Lorentzian linewidth is measured by placing a marker at the half power frequency.

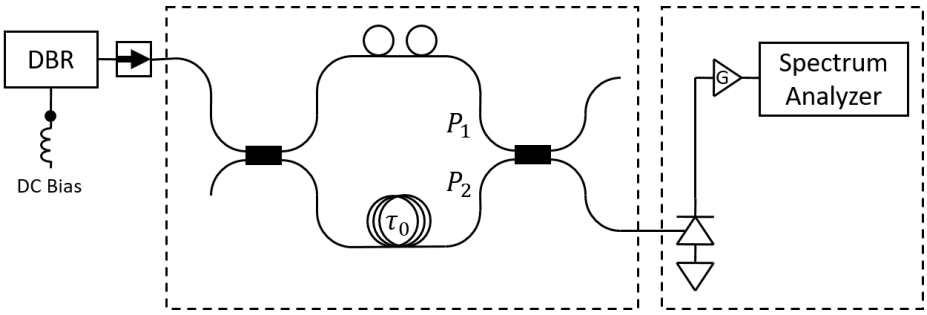

Figure 3.5.: Schematic set-up for self-homodyne linewidth measurement.

The results of linewidth measurement are shown in Figure 3.6. Except for the unstable working points which are shown in light grey in Figure 3.6 (a), the laser linwidth under

feedback become narrower than the case without feedback. It is due to the reason that the external refelctor formed by the polymer/air interface with $r_{ext} = 0.187$ is considered to be in the strong feedback region. In such case, the practical formula for linewidth reduction factor F^2 Equation 2.15 has to be considered. The comparison for the lowerest linewidth for each configuration, along with the theoretical predcition, is shown in Table 3.1.

Table 3.1.: Comparison of the linewidth reduction value achieved by laser w/ and w/o feedback, and the predicated reduction value.

	Cleaved with oil	Lensed	Reduction	Reduction (Predicated)
$\Delta\nu$ (MHz)	0.522 @ Index 52	0.317 @ Index 4	1.647	1.11

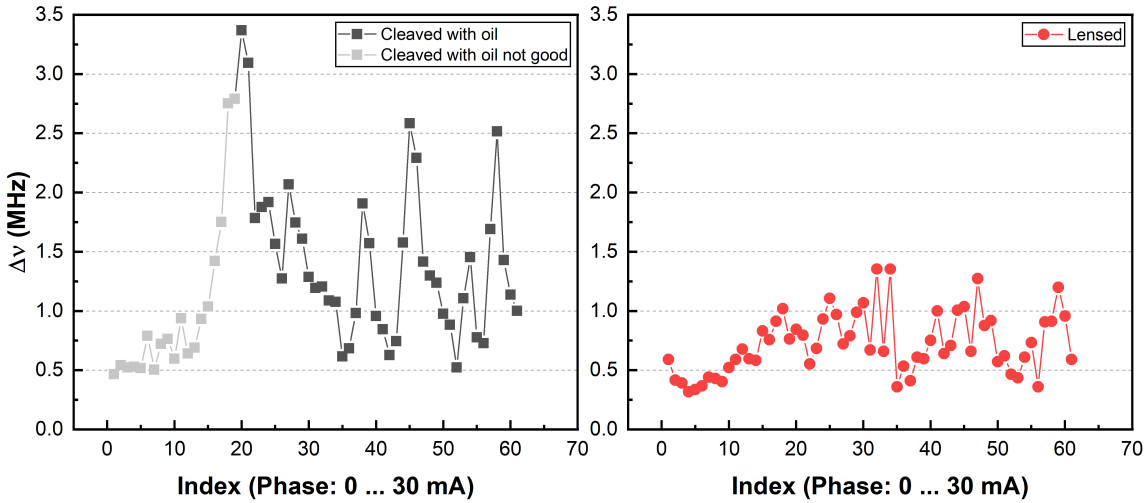

Figure 3.6.: (a) The laser linewidth without feedback from the chip facet, the light grey points indicate the bad working points, (b) laser linewidth with feedback from the chip facet, it shows a more stable behavior compare to the laser without feedback.

3.2. Relative Intensity Noise (RIN) Measurement

The measurement of relative intensity noise (RIN) describes the laser's maximum available range for signal modulation and serves as a quality indicator of laser devices. RIN is defined as the ratio of the mean-square optical intensity noise to the square of the average optical power: [cite]

$$RIN = \frac{\langle \Delta P \rangle^2}{\langle P \rangle^2} dB/Hz \tag{3.1}$$

where $\langle \Delta P \rangle^2$ is the mean-square optical intensity fluctuations (in a 1-Hz bandwidth) at a specified frequency, and $\langle P \rangle$ is the mean optical power.

In order to measure the RIN, the optical power is converted to a current after the receiving photodiode and the ratio of optical powers squared is equivalent to the ratio of the detected electrical powers. Thus, RIN can be expressed in terms of detected electrical powers. Equation 3.1 can be rewritten as:

$$RIN = \frac{N_{elec}}{P_{avg}(elec)}\ dB/Hz \tag{3.2}$$

where N_{elec} is the power-spectral density of the photocurrent at a specified frequency, and $P_{avg}(elec)$ is the average power of the photocurrent.

The noise at the receiver output results from three fundamental contributions: laser intensity noise primarily due to spontaneous light emissions; thermal noise from the electronics; and photonic shot noise. Since the photonic shot noise and the receiver thermal noise are not included in the definition of N_{elec}, they have to be subtracted from the measured RIN results:

$$N_{laser} = N_{elec} - N_{shot} - N_{thermal}\ W/Hz \tag{3.3}$$

By using Equation 3.2 and Equation 3.3, the value of RIN_{laser} can be determined:

$$RIN_{laser} = RIN(measured) - \frac{2e}{I_{avg}} - \frac{N_{thermal}}{P_{avg}(elec)} \tag{3.4}$$

where e is the elementary charge, I_{avg} denotes the detected average photocurrent, $N_{thermal}$ is the measured noise floor of the lightwave signal analyzer in a 1-Hz bandwidth.

The RIN comparison for the two configurations are shown in Figure 3.7. The RIN value for laser w/o feedback ranges from -144 dB/Hz to -142 dB/Hz while for lase w/ feedback it has two parts: without the spikes it ranges from -146 dB/Hz to -144 dB/Hz, which is lower than the case w/o feedback; the spikes appear in Figure 3.7 (b) are correspoinding to the additional mode hopping behavior in Figure 3.3 (b), which indicates the appearing of the undamped RO, will increase the RIN value.

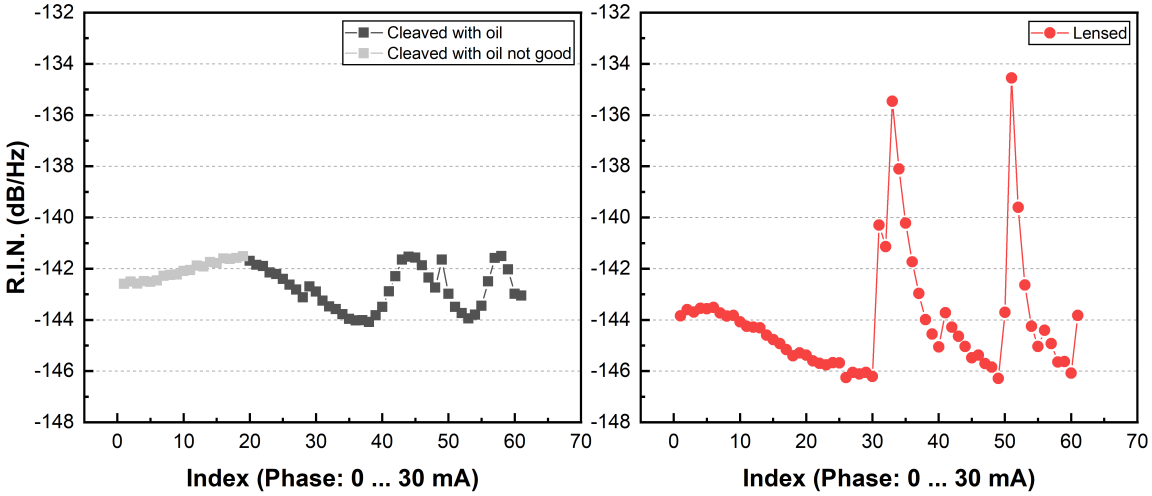

Figure 3.7.: Comparison of the RIN value for laser w/ and w/o feedback. (a) Laser with feedback, (b) laser without feedback, the spikes indicate the appearing of the undamped RO, which increase the RIN significantly.

3.3. Bandwidth Measurement

3.3.1. Small Signal Modulation

From a practical viewpoint the quantity of interest is the modulation bandwidth ν_B which indicates the frequency range over which the laser responds to the current modulation. It is usually defined as the frequency at which the modulation response has dropped by 3 dB relative to its low-frequency or DC value [21].

The frequency response of the laser transmitter under small signal modulation is found by the usual assumption of a harmonic current modulation superimposed on a constant bias above threshold.

$$H(\omega) = \frac{\omega_R^2}{\omega_R^2 - \omega^2 - 2j\omega\gamma} \tag{3.5}$$

in Equation 3.5, ω_R is the relaxation resonance frequency and γ is the damping factor.

The relaxation oscillation frequency is a measure of the maximum modulation ability in semiconductor lasers through the injection current. Above the relaxation oscillation, the modulation efficiency is greatly degraded and intensity modulation through the injection current becomes difficult. [Semiconductor Lasers. Stability, Instability and Chaos.pdf]

The laser seeks a steady-state operation which maximizes feedback. When external feedback is present, the state corresponding to maximum feedback occurs when there is phase alignment between the semiconductor cavity field and the reflected field. A carrier number change n will change the resonance frequency of the semiconductor cavity. This in turn causes a phase change ϕ between the laser field and the reflected field. This acts to decrease the light intensity in proportion to $1 - cos\phi \approx \frac{\phi^2}{2}$, which decreases the rate of stimulated emission and further increases n. This increase in n again raises the cavity resonance frequency, causing the phase misalignment ϕ to continue to grow. Instability occurs for finite fluctuations of ϕ

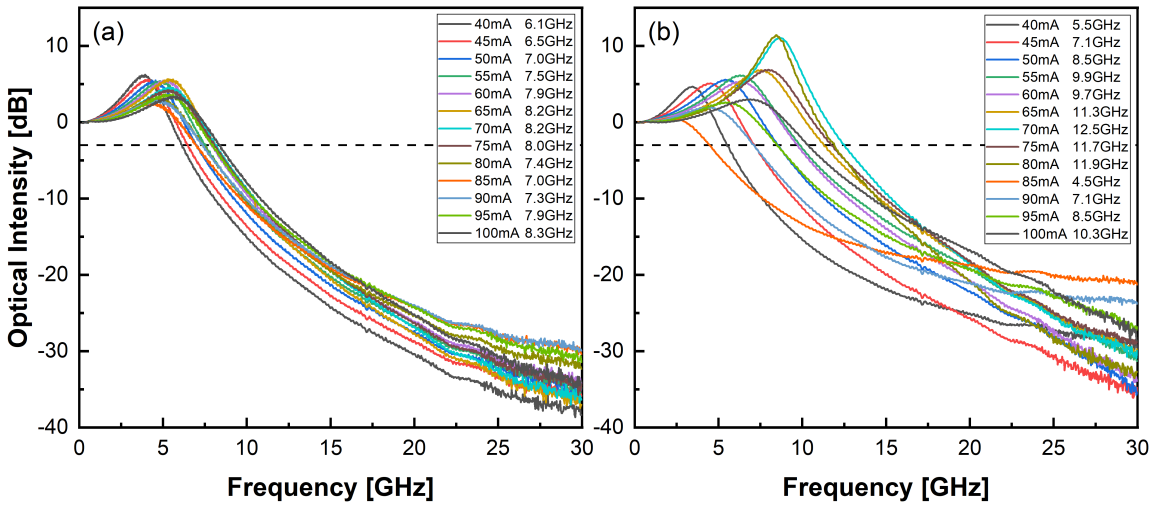

Figure 3.8.: Bandwidth measurements of a normal tunable laser. (a): Without feedback, the f_{3dB} show a normal behavior that first increase with the applied gain current and then decrease, (b): with feedback, the prominant peaks at 70 mA and 75 mA are due to the undamped RO peaks, at this condition, the f_{3dB} got increased compare with the lase without feedback.

and n when this effect becomes greater than the restoring forces giving rise to the relaxation oscillations described above.

steady-state operation (phase alignment of the cavity field and reflected field)

In steady-state operation, the laser with reflective feedback can be thought of as phase locked to the reflected field. The phenomenon that we describe is driven by large fluctuations in spontaneous emission that dislodge the laser from this locked state that is stable for small fluctuations. [Henry, Kazarinov 1986]

3.3.2. Detuend loading condition

Operating the DBR laser under the detuned loading condition was measured and the result is shown in Figure 3.9. The measurement was performed by stabilizing the device at 25 °C and using a gain current I_{gain} of 75 mA. When the laser is lasing on the slope of the grating response, the side modes have a different gain spectrum relative to the peak of the grating response, which introduces the asymmetric behavior of the side modes. In this case, when the left side mode is higher than the right one, means the lasing mode is operating at the longer wavelength side of the grating response, and vice versa. By increasing the phase current I_{phase} from 14 mA to 20 mA, the lasing mode is tuned from the longer wavelength side of the grating response to the shorter wavelength side. The maximum f_{3dB} achieved at the longer wavelength side (red curve in Figure 3.9) is 10.6 GHz and the minimum (grey curve in Figure 3.9) is 8.5 GHz.

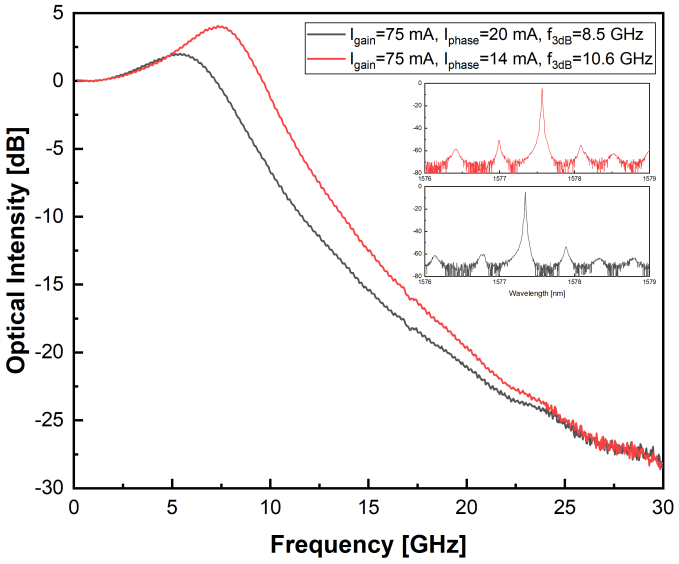

Figure 3.9.: Bandwidth enhancement with the detuned loading condition on DBR tunable laser. The red curve is detuned to the longer wavelength side of the grating response, shows an increased bandwidth of 2.1 GHz compared to the grey curve without bandwidth enhancement effect.

3.3.3. Undamped RO

For the laser under undamped RO conditions, not all the undamped behavior lead to the good performance of the laser. As shown in Figure 3.10, the appearing of the undamped RO peak leads to the carrier-photon resonance appears at a higher relaxation oscillation frequency which permits a higher f_{3dB} value. As the side peaks slowly move towards the main peak with increasing intensity, the carrier-photon resonance become stronger with a slightly decreased relaxation oscillating frequency. When more side peaks appear in Figure 3.10 (c.1), the undamped RO behavior is very strong which lead to a broder lineshape and the intensity modulation shows prominent peaks with frequency correspoinding to the mode spacing of the side peaks. This last behavior leads to broadened lineshape and significantly decreases the f_{3dB} compare to the other two cases.

3.3.4.

Chirp arises because the frequency of the laser mode depends on the carrier number in the active region. Above threshold, the carrier number changes because of two effects: spectral hole burning prohibits the perfect pinning of the carrier number and permits adiabatic chirp, and during transients, there are relaxation oscillations of carrier number, which cause dynamic chirp. [Kazarinov 1987]

Current modulation of the active region results in a modulation of both the photon density and the carrier density. The modulation of the carrier density modulates the gain; however, it also modulates the index of the active region na . As a result, the optical length of the cavity

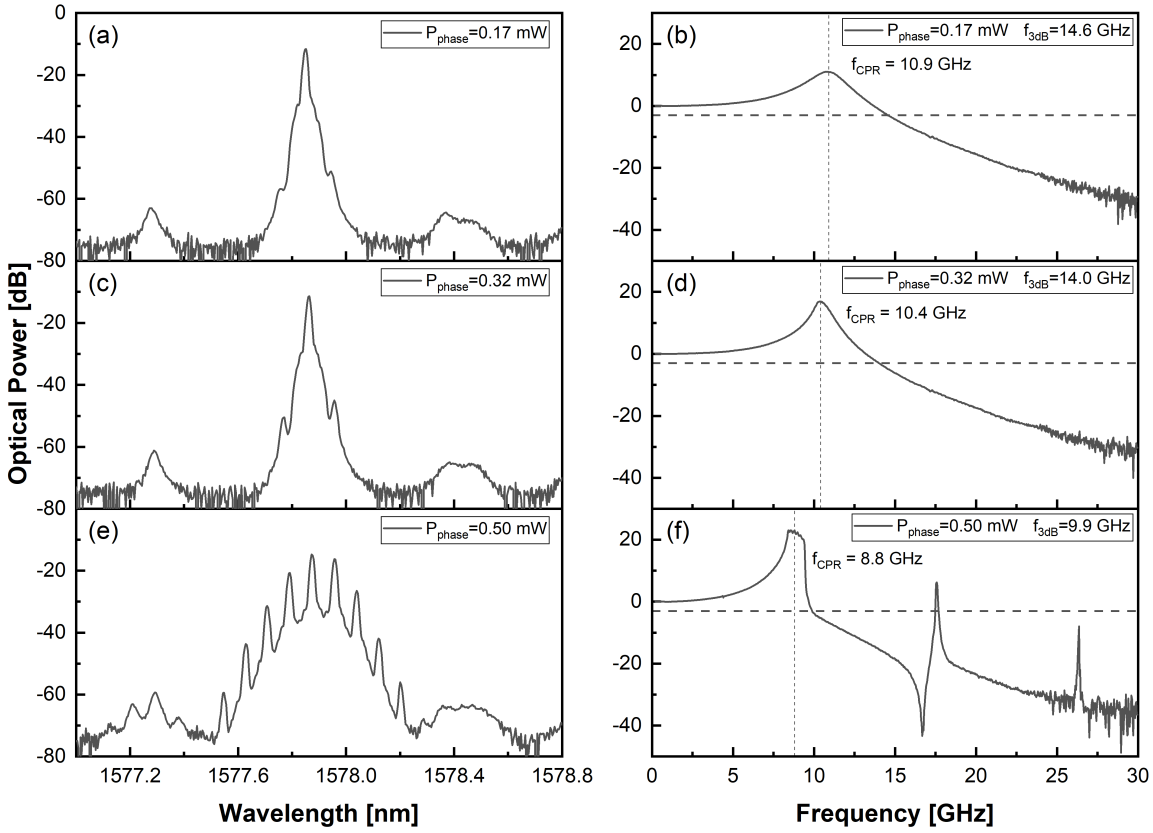

Figure 3.10.: Laser spectra and their correspoinding intensity modulation curve. (a) Appearing of the undamped RO peak leads to a higher carrier-photon resonance in (b), (c) growing of the side peaks leads to increase of the carrier-photon resonance peak in (d), (e) drastic undamped RO leads to broadened lineshape and decreased modualiton bandwidth in (f).

is modulated by the current, causing the resonant mode to shift back and forth in frequency. [Larry A. Coldren.pdf]

If we consider the case discussed earlier where the semiconductor cavity is extended by a passive section of length L_1, with a nonreflective transition between the two sections, the reflection at the semiconductor section constant in magnitude, but has a frequency-dependent phase shift with $d\phi_r/d\omega = 2L_1/v_g1$ where $2L/v_g1$ is the roundtrip time in the external cavity. Therefore, in this case $B = 0$, the chirp reduction factor is [Kazarinov 1987]

3.4. Chirp Parameter Measurement

(α-Factor) Light chirping is a parasitic property of intensity modulated light. It originates in light emitters that produce a phase shift as the intensity is varied [22]. Semiconductor lasers exhibit a particular nonlinearity in the interaction of the light with the active

medium, which distinguishes them from all other lasers. The nonlinearity originates from the physics of the semiconductor band structure, since the photon generation typically occurs due to interband transitions. The gain spectrum of such lasers therefore does not exhibit a symmetric peak, as atomic transitions do, but has a strongly asymmetric shape. This affects the dispersive properties of the lasers as well, since those properties are connected via the Kramers-Kronig relation. As a consequence, the dispersion curve for the refractive index exhibits its zero crossing at higher frequency than the maximum of the gain spectrum. If the gain changes, e.g., by a change of the carrier density, the refractive index changes as well, which would not be the case for atomic transitions. Hence, changes in gain are in semiconductor lasers associated with changes in refractive index and vice versa. Since with a change of refractive index of the medium the optical frequency and thus the optical phase changes, one also speaks of amplitude phase coupling. A small change in the intensity (induced, e.g., by a change in the injection current, by dynamical instabilities, or even a spontaneous emission event) causes an excess perturbation of the phase of the lasing mode. In the rate equation description, the effect is taken into account via the so-called α parameter, which is also referred to as Henry parameter or linewidth enhancement factor. It is defined as

$$\alpha = -\frac{d\chi_r(n)/dn}{d\chi_i(n)/dn} \tag{3.6}$$

3.4.1. Measurement with LCA

The network analyzer of Figure 3.11 measures the small-signal frequency response of a light emitter, a dispersive medium and a light receiver. The dispersive medium is 81 km of standard, single-mode fiber (zero dispersion at 1.3 μm) from and Er-doped fiber amplifiers pumped at 1.55 μm. Resonance frequencies are observed as sharp peaks in the frequency response.

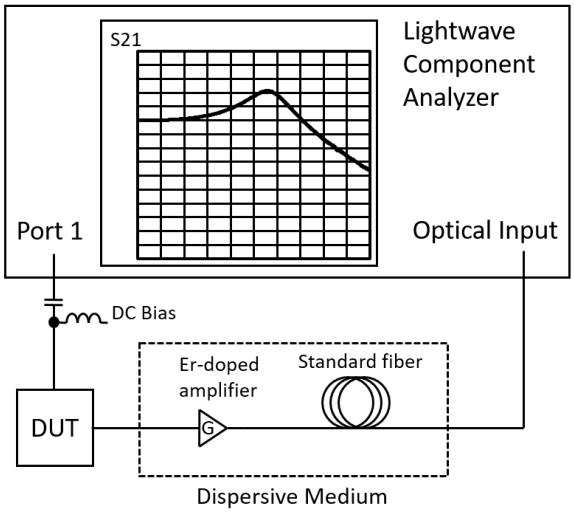

Figure 3.11.: Schematic set-up for chirp parameter measurement.

The resonance frequencies f_u of Fig.2 corresponds to the u^{th}-zeros of xx. They follow a very simple law:

$$f_u^2 L = \frac{c}{2D\lambda^2}(1 + 2u - \frac{2}{\pi}arctan(\alpha)) \tag{3.7}$$

The equation is the result of two simultaneous interferences between the carrier and the two sidebands. Plotting $f_u^2 L$ versus $2u$ gives a straight line whose slope and position yield the dispersion and the chirp parameter by liner regression.

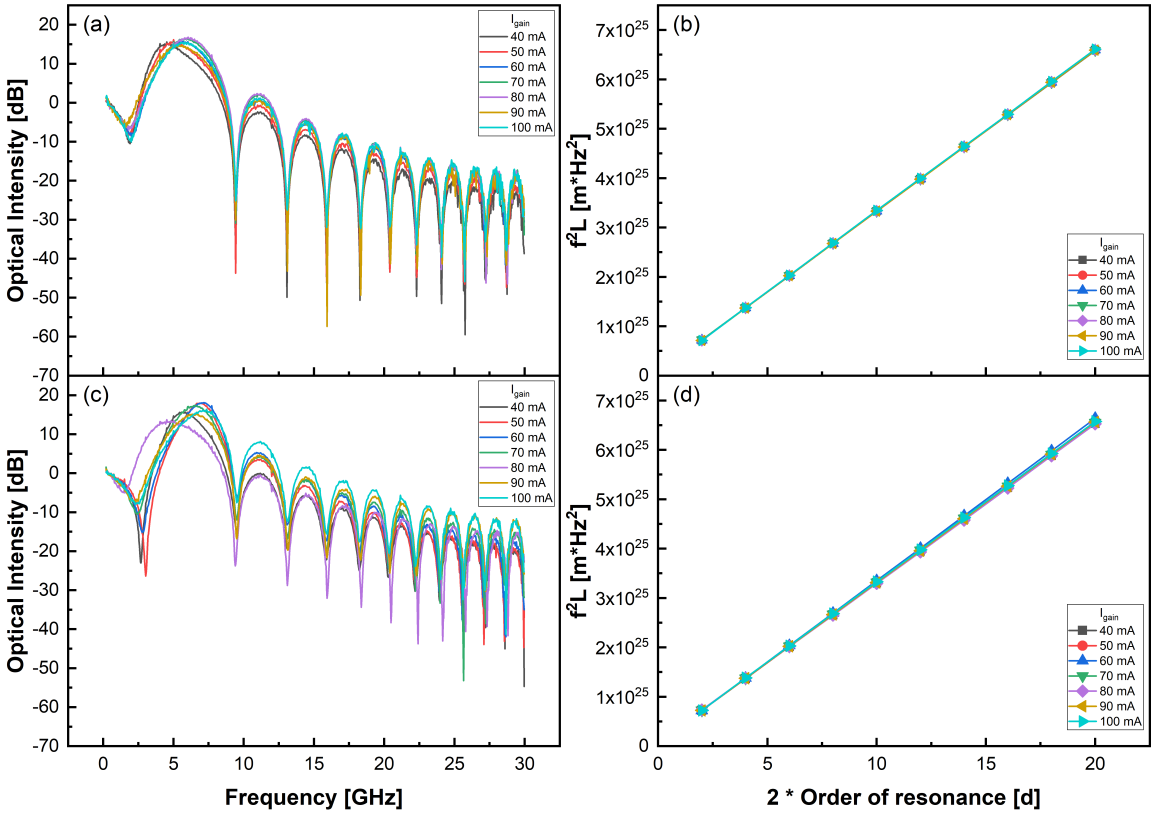

Figure 3.12.:

3.4.2. AM-FM Index Method

The experimental arrangement for measuring the intensity and phase modulation index is shown in Fig. 1. The semiconductor laser is biased above threshold and a small sinusoidally varying current at frequency Ω is superimposed. The intensity and spectral density of the radiation field are given by

$$Intensity : E_0^2[1 + mcos(\Omega t)] \tag{3.8}$$

$$Spectrum : Center\ line\ at\ \omega_1 : E_0^2[J_0^2(\beta) + m^2 J_1^2(\beta)] \tag{3.9}$$

$$First\ sidebands\ at\ \ \omega_1 \pm \Omega : E_0^2\left\{J_1^2(\beta) + 1[(m/2)(J_2(\beta) - J_0(\beta))]^2\right\} \tag{3.10}$$

Table 3.2.: My caption

Current [mA]	α	
	w/o feedback	w/ feedback
40	3.164	2.499
50	3.017	2.247
60	2.687	2.439
70	3.079	2.593
80	3.003	3.095
90	2.996	2.389
100	2.605	2.472

The phase modulation index β can be found by measuring the relative sideband strength and using Equation 3.9 and Equation 3.10. The factor α_m is then obtained as $\alpha_m = -2(\beta/m)$.

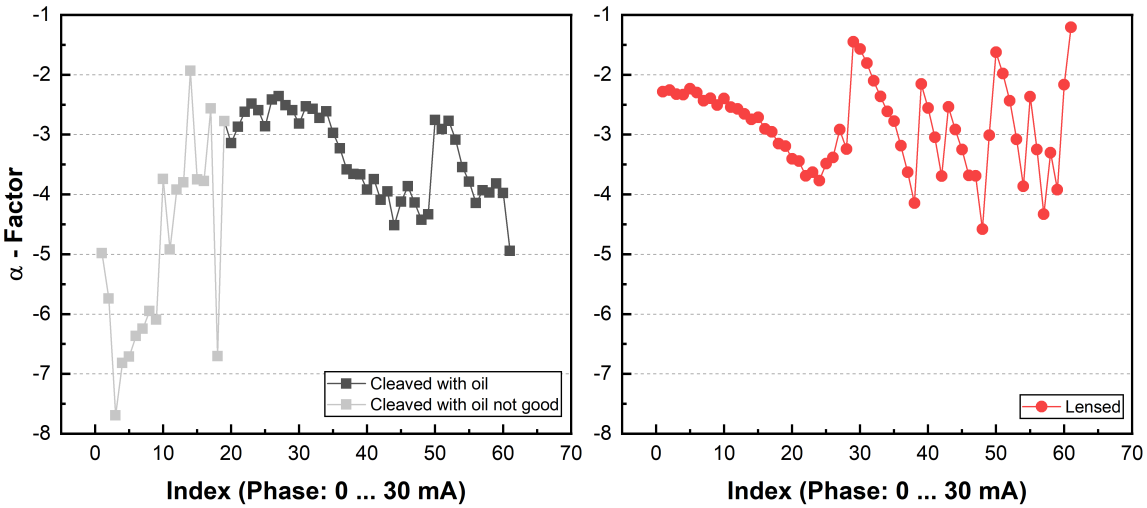

Figure 3.13.: Comparison of α parameter

3.5. Phase Noise Measurement

4. Tunable Laser with on Chip Controllable Feedback

4.1. Design

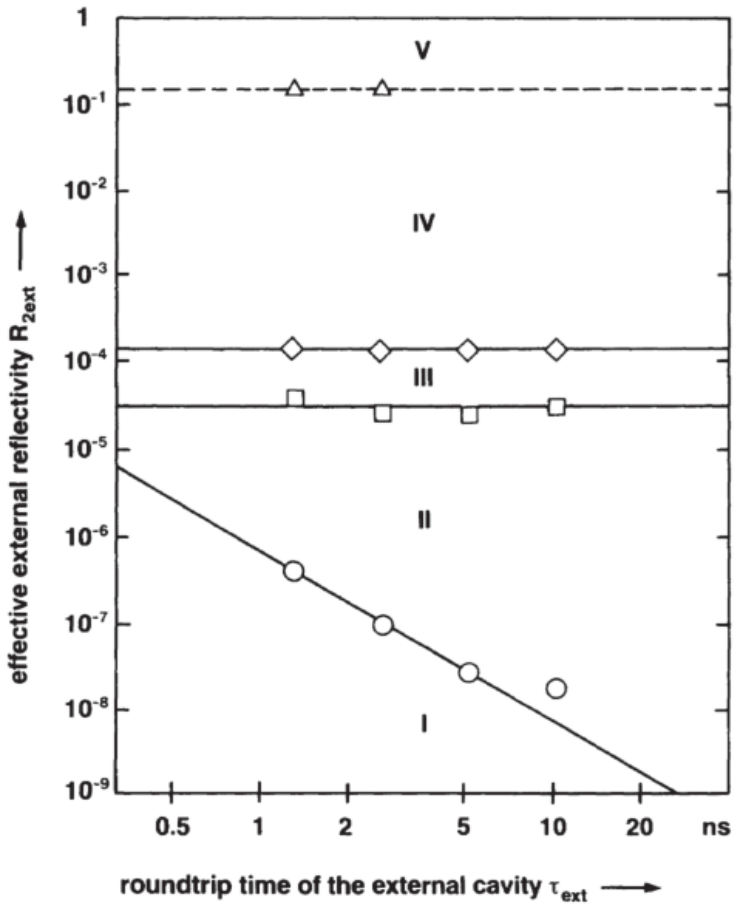

Figure 4.1.: Feedback regimes for a laser diode.

4.1.1. Active and Passive Elements

As a variable optical attenuator (VOA) a 1x1 thermally tunable Multimode interferometer (MMI) is used (Fig.3.4.c). MMI is a multimode waveguide in which the light propagates

in N modes. The various modes interfere with each other and produce an interference pattern in the MMI. This pattern allows at points of constructive interference to place output waveguide and thus to tap multiple outputs, each with a corresponding proportion of the total output power from an input signal. Depending on the design of the structure, the MMI can realize a different power division. On one side along the MMI is placed an electrode that allows using the thermo-optical effect. We distinguish the states ON and OFF. In the OFF state, there is no heating of the electrodes and constructive interference takes place at the point where the output waveguide is. In ON-state, the interference pattern of the MMI is so affected, so that shifts through the partial change of the refractive index of the MMI, the position of constructive interference. Thus, a maximum interference point moves away from the position of the output waveguide and the output signal is tapped at reduced power (Fig.3.4.a and b). In this way a variable optical attenuation is created. An input waveguide with a width and height of 3.2 µm leads light into the interferometer. The height of the MMI (x-axis) also corresponds to 3.2 µm, the width is 18 µm and the length is 380 µm. The light that is leaving the MMI is received by an output waveguide. Height and width of the output waveguide coincide with the dimensions of the input waveguide. The transition of the input and output waveguide of the MMI is realized with taper sections that reduce the coupling losses. This VOA design was showing the best results compare to the literature [16-18].

4.1.2. Long Feedback Cavity

4.1.3. Short Feedback Cavity

4.2. Characterization

Table 4.1.: My caption

Current [mA]	α				
	$I_{phase} = 10\ mA$	$I_{phase} = 11\ mA$	$I_{phase} = 12\ mA$	$I_{phase} = 13\ mA$	$I_{phase} = 14\ mA$
75	1.725	2.063	2.22	2.624	3.247
75	1.818	1.991	2.296	2.618	3.257
75	1.818	2.07	2.246	2.614	3.253
75	1.808	2.054	2.242	2.566	3.221
Average	1.79225	2.0445	2.251	2.6055	3.2445

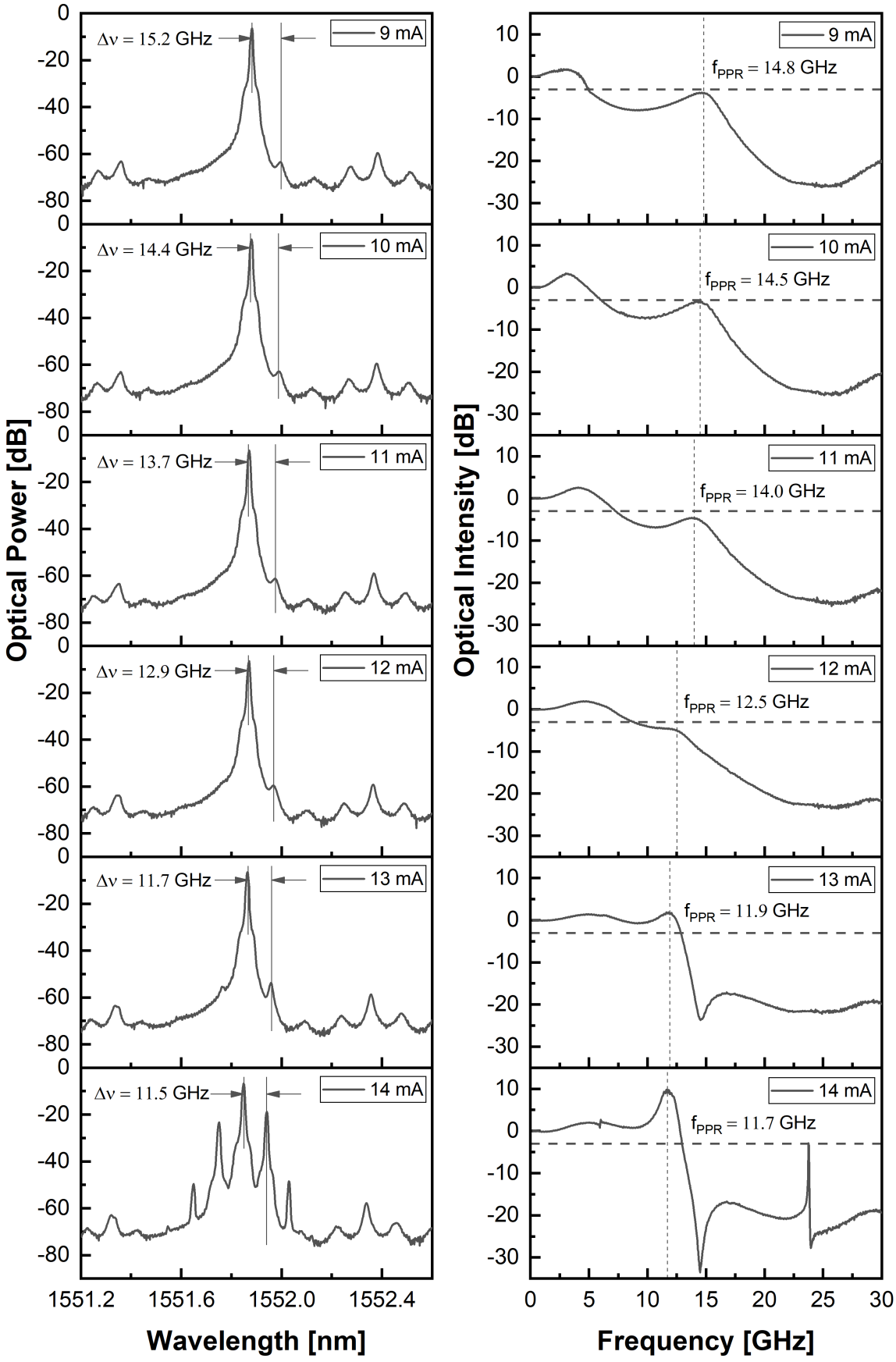
Optical Power [dB]
Δν = 15.2 GHz
9 mA
Δν = 14.4 GHz
10 mA
Δν = 13.7 GHz
11 mA
Δν = 12.9 GHz
12 mA
Δν = 11.7 GHz
13 mA
Δν = 11.5 GHz
14 mA
Wavelength [nm]
Optical Intensity [dB]
f_PPR = 14.8 GHz
f_PPR = 14.5 GHz
f_PPR = 14.0 GHz
f_PPR = 12.5 GHz
f_PPR = 11.9 GHz
f_PPR = 11.7 GHz
Frequency [GHz]

Figure 4.2.:

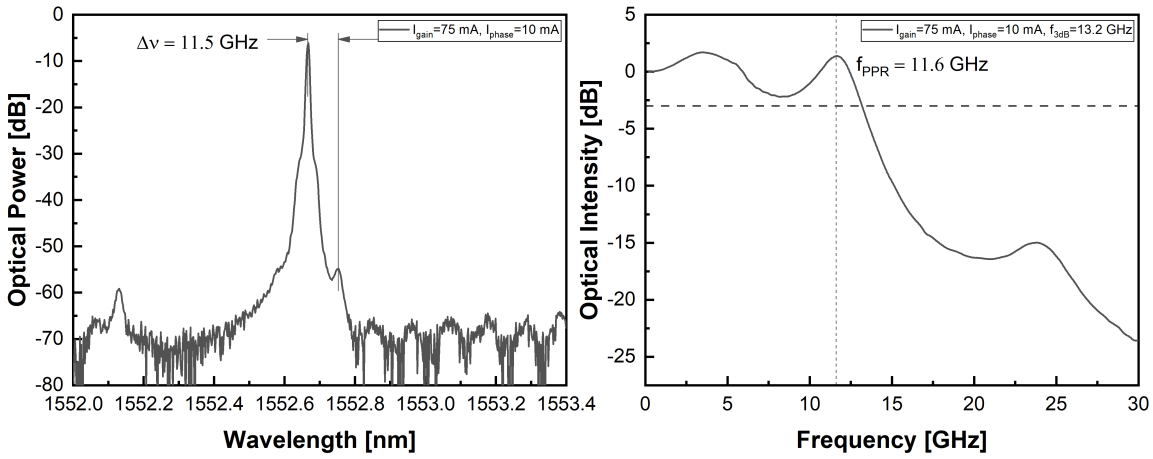

Figure 4.3.:

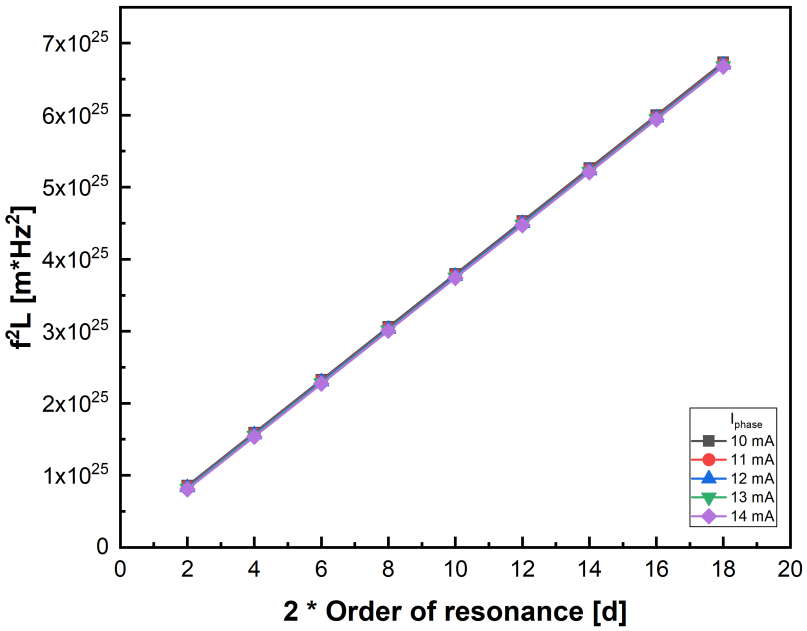

Figure 4.4.:

5. Conclusions & Outlook

5.1. Conclusions

5.2. Outlook

Bibliography

[1] Miguel C Soriano et al. "Complex photonics: Dynamics and applications of delay-coupled semiconductors lasers". In: *Reviews of Modern Physics* 85.1 (2013), p. 421.

[2] Mark Kuznetsov. "Theory of wavelength tuning in two-segment distributed feedback lasers". In: *IEEE journal of quantum electronics* 24.9 (1988), pp. 1837–1844.

[3] Daan Lenstra, B Verbeek, and A Den Boef. "Coherence collapse in single-mode semiconductor lasers due to optical feedback". In: *IEEE Journal of Quantum Electronics* 21.6 (1985), pp. 674–679.

[4] R Tkach and AR Chraplyvy. "Regimes of feedback effects in 1.5-μm distributed feedback lasers". In: *Journal of Lightwave technology* 4.11 (1986), pp. 1655–1661.

[5] Amnon Yariv and Michiharu Nakamura. "Periodic structures for integrated optics". In: *IEEE Journal of Quantum Electronics* 13.4 (1977), pp. 233–253.

[6] Marco Vallone, Paolo Bardella, and Ivo Montrosset. "Enhanced modulation bandwidth in complex cavity injection grating lasers". In: *IEEE Journal of Quantum Electronics* 47.10 (2011), pp. 1269–1276.

[7] Larry A Coldren, Scott W Corzine, and Milan L Mashanovitch. *Diode lasers and photonic integrated circuits*. Vol. 218. John Wiley & Sons, 2012.

[8] R Kazarinov and C Henry. "The relation of line narrowing and chirp reduction resulting from the coupling of a semiconductor laser to passive resonator". In: *IEEE Journal of quantum electronics* 23.9 (1987), pp. 1401–1409.

[9] Klaus Petermann. *Laser diode modulation and noise*. Vol. 3. Springer Science & Business Media, 2012.

[10] Kerry Vahala and Amnon Yariv. "Detuned loading in coupled cavity semiconductor lasers—effect on quantum noise and dynamics". In: *Applied Physics Letters* 45.5 (1984), pp. 501–503.

[11] Kerry Vahala, Joel Paslaski, and Amnon Yariv. "Observation of modulation speed enhancement, frequency modulation suppression, and phase noise reduction by detuned loading in a coupled-cavity semiconductor laser". In: *Applied Physics Letters* 46.11 (1985), pp. 1025–1027.

[12] Uwe Feiste. "Optimization of modulation bandwidth in DBR lasers with detuned Bragg reflectors". In: *IEEE journal of quantum electronics* 34.12 (1998), pp. 2371–2379.

[13] Olle Kjebon et al. "Two-section InGaAsP DBR-lasers at 1.55/spl mu/m wavelength with 31 GHz direct modulation bandwidth". In: *Indium Phosphide and Related Materials, 1997., International Conference on*. IEEE. 1997, pp. 665–668.

[14] Marek Chacinski and Richard Schatz. "Impact of losses in the Bragg section on the dynamics of detuned loaded DBR lasers". In: *IEEE Journal of Quantum Electronics* 46.9 (2010), pp. 1360–1367.

[15] Olle Kjebon et al. "Experimental evaluation of detuned loading effects on distortion in edge emitting DBR lasers". In: *IEEE International Topical Meeting on Microwave Photonics pp.* 2002, pp. 125–128.

[16] Junji Ohtsubo. *Semiconductor lasers: stability, instability and chaos*. Vol. 111. Springer, 2012.

[17] U Bandelow, HJ Wunsche, and H Wenzel. "Theory of selfpulsations in two-section DFB lasers". In: *IEEE photonics technology letters* 5.10 (1993), pp. 1176–1179.

[18] Richard Schatz et al. "Enhanced modulation bandwidth and self-pulsations in detuned loaded InGaAsP DBR-lasers". In: *Semiconductor Laser Conference, 1996., 15th IEEE International*. IEEE. 1996, pp. 93–94.

[19] Ivo Montrosset and Paolo Bardella. "Laser dynamics providing enhanced-modulation bandwidth". In: *Semiconductor Lasers and Laser Dynamics VI*. Vol. 9134. International Society for Optics and Photonics. 2014, 91340H.

[20] JP Reithmaier et al. "Modulation speed enhancement by coupling to higher order resonances: a road towards 40 GHz bandwidth lasers on InP". In: *Indium Phosphide and Related Materials, 2005. International Conference on*. IEEE. 2005, pp. 118–123.

[21] Govind P Agrawal and Niloy K Dutta. *Semiconductor lasers*. Springer Science & Business Media, 2013.

[22] F Devaux, Y Sorel, and JF Kerdiles. "Simple measurement of fiber dispersion and of chirp parameter of intensity modulated light emitter". In: *Journal of Lightwave Technology* 11.12 (1993), pp. 1937–1940.

A. Appendix

A.1. Photon-photon resonance calcuation